J Mater Sci (2008) 43:117–122
DOI 10.1007/s10853-007-2086-8

High-aspect ratio polymeric pillar arrays formed via electrohydrodynamic patterning

Michael D. Dickey · Allen Raines · Elizabeth Collister · Roger T. Bonnecaze · S. V. Sreenivasan · C. Grant Willson

Received: 18 April 2007 / Accepted: 6 August 2007 / Published online: 26 September 2007
© Springer Science+Business Media, LLC 2007

Abstract This paper describes a method to increase the aspect ratio of polymeric pillar arrays formed by electrohydrodynamic instabilities. Pillar arrays form spontaneously across a narrow capacitor gap when an electric field is applied normal to a thin, fluidic film. This simple technique is appealing because of its ability to rapidly form arrays of small structures in an inexpensive manner. The columnar structures formed using this technique have low-aspect ratios, which are non-ideal for patterning applications. Theory suggests that stretching the structures post-formation is one of the only ways to increase the aspect ratio of the pillars. We developed a tool to physically stretch these structures to increase their aspect ratio from $\sim$0.1 to $\sim$0.5. The capabilities and limits of this stretching technique have been discussed.

Introduction

Patterning techniques are often sought to overcome the intrinsic limitations of photolithography, such as resolution, cost, and material restrictions. Recently, a simple, low-cost patterning technique was demonstrated that utilizes electrohydrodynamic instabilities to form arrays of polymeric pillars [1–3]. Pillars spontaneously form across a narrow gap when a thin-film is destabilized by an electric field. This directed-assembly lithographic approach is appealing because of its simplicity and ability to rapidly produce arrays of small structures in an inexpensive manner. Structures formed by this technique are typically micron scale, although features as small as 100 nm have been demonstrated through the use of patterned electrodes [1].

The columnar structures formed using this technique have low-aspect ratios (height:diameter), although high-aspect ratio features are generally preferable for patterning applications. Patterned features often serve as sacrificial materials to protect the underlying surface during subsequent processing (e.g., etching, ion bombardment). High-aspect ratio features protect the substrate more effectively than low-aspect ratio features. In addition, harvestable high-aspect ratio pillar structures may have attractive properties when placed in solution or when used in composite materials.

We developed a machine—the active gap tool—to increase the aspect ratio of the pillars via stretching. The active gap tool positions a flat, conductive plate (i.e., the upper electrode) above a film-coated substrate to create a small, uniform air gap. Pillars form when an electric field is applied across the gap. The tool stretches the pillars by withdrawing the template in a controlled manner. This article discusses the design, capabilities, and limits of the active gap tool as an approach to form high-aspect ratio pillar arrays.

Theory

Pillars form due to the amplification of thin-film undulations induced by a destabilizing force, such as an electric

M. D. Dickey · E. Collister · R. T. Bonnecaze · C. G. Willson (✉)
Department of Chemical Engineering, University of Texas at Austin, Austin, Texas 78712, USA
e-mail: willson@che.utexas.edu

A. Raines · S. V. Sreenivasan
Department of Mechanical Engineering, University of Texas at Austin, Austin, Texas 78712, USA

field. Figure 1 illustrates the process used to form pillars. A flat, conducting electrode is brought within proximity of a thin-film coated substrate. The resulting gap resembles a capacitor, across which an electric field may be applied. Pillars form if the electrostatic force acting at the film interface is strong enough to overcome the stabilizing effects of surface tension. The force imbalance amplifies film fluctuations until the undulations span the capacitor gap to form pillars. The fluidic pillars can be solidified by photopolymerization; this approach requires a transparent upper electrode.

Unfortunately, pillars formed by electrohydrodynamic instabilities have low-aspect ratios, defined as the ratio of the height to the diameter of the pillar. A recent literature survey shows that polymeric pillar arrays typically have aspect ratios between 0.05 and 0.2 [4]. We have observed similar aspect ratios in a number of photocurable materials [5]. Figure 2 is a representative tilt-view scanning electron micrograph (SEM) of photocured pillars on a silicon substrate with aspect ratios of $\sim$0.1.

The theoretical aspect ratio can be derived by combining the characteristic spacing of the structures (i.e., pillar center-to-center spacing) with conservation of mass. Linear stability analysis is typically utilized to predict the characteristic spacing and its applicability has been verified experimentally [1, 3, 4, 6–11]. The characteristic spacing, λ, is defined in Eq. 1 [1].

$$\lambda = 2\pi \frac{(2\gamma)^{1/2}(\varepsilon(d-h)+h)^{3/2}}{|V|(\varepsilon\varepsilon_0)^{1/2}(\varepsilon-1)} \tag{1}$$

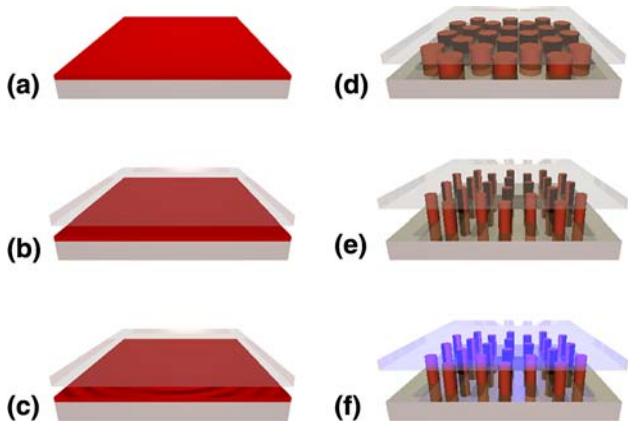

Fig. 1 The pillar formation and stretching process. (**a**) A thin film is cast onto a silicon substrate. (**b**) The active gap tool positions a transparent and conducting electrode above the film, forming a small gap. (**c**) An electric field applied across the gap causes the film to become unstable. (**d**) Undulations in the film amplify until they span the capacitor, forming pillars. (**e**) The active gap tool stretches the pillars. (**f**) Ultraviolet light irradiated through the upper electrode cures the resulting structures

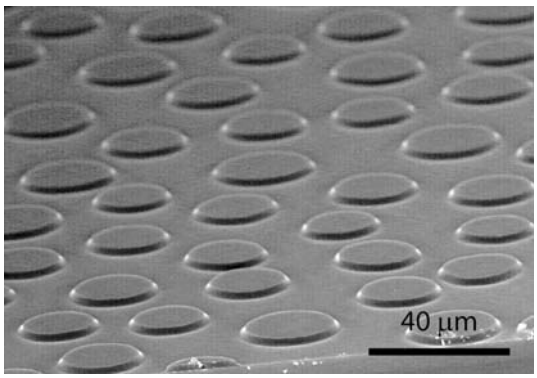

Fig. 2 Tilt-view SEM of polymeric pillars (formed using 40 V, 2.5 µm gap, 800-nm film). The pillars have low-aspect ratios ($\sim$0.1), typical of the pillar formation process

where V is the voltage, ε is the dielectric constant of the film, ε_0 is the permittivity of free space, h is the undisturbed film height, and γ is surface tension.

Assuming all of the initially undisturbed film is entrained into the pillars, a simple mass balance provides the aspect ratio (Eq. 2). This assumption appears valid for the materials used in this study based on experimental observation [5].

$$\frac{H}{D} = \left[\frac{\pi d^3}{4\lambda^2 h}\right]^{1/2} \tag{2}$$

where D is the average diameter of the pillars and H is the height of the pillar, which is equivalent to the electrode gap, d. An examination of Eq. 2 reveals several approaches to increase the aspect ratio: The overall gap can be increased, the film height decreased, or the characteristic spacing decreased. The characteristic spacing is minimized by increasing the electrostatic force and decreasing the surface tension. As implied by Eq. 1, these forces depend on both h and d, as well as the material properties of the film (ε and γ) and the applied voltage, V. Therefore, for a given material, the aspect ratio is a function of three independent variables: V, d, and h. These three variables can be accounted for by plotting the aspect ratio as a function of the fill factor (the ratio of film height, h, to the electrode gap, d) for a particular electric field (V/d), as shown in Fig. 3.

The aspect ratio is a function of the electric field. Large electric fields maximize the destabilizing force acting at the interface, favoring structures with smaller characteristic spacing. Unfortunately, the electric field cannot be increased past the dielectric breakdown of the capacitor; this occurs between the experimentally observed values of 50–80 V/µm. Despite plotting the most favorable electric field (50 V/µm) in Fig. 3, the aspect ratios are below 0.5 for most fill factors.

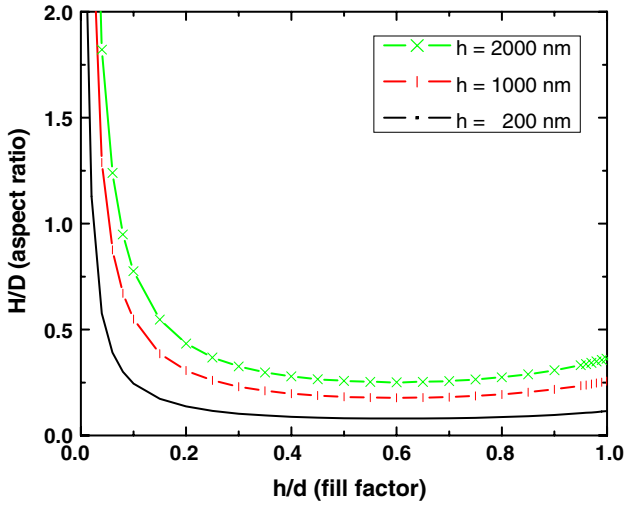

Fig. 3 Theoretical aspect ratio versus fill factor for several film thicknesses. The plot assumes the largest physical electric field possible (50 V/μm), which favors large aspect ratios (assumes a material with $\varepsilon = 3$, $\gamma = 40$ mJ/cm^2)

The aspect ratio is also a function of the electrode gap, d. The effect of varying d for intermediate fill factors, however, is negligible since λ scales with $d^{3/2}$ (and thus the λ and d terms in Eq. 2 effectively cancel). The theoretical aspect ratio is enhanced at the extreme values of the fill factor ($h/d \sim 0$ and $h/d \sim 1$), although these values are problematic in practice. Recent modeling has shown that large fill factors lead to pillar coalescence and small fill factors have exceedingly large time scales of pillar formation [10]. Consequently, pillar formation usually occurs at intermediate fill factors, leading to low-aspect ratios (e.g., Fig. 2).

The aspect ratio is also a function of film height. The linear stability analysis used to predict the characteristic spacing, however, is only valid for thin films ($h/\lambda << 1$); thus the aspect ratio cannot be increased significantly through the use of thick films.

The aspect ratio can be increased through the use of a topographically patterned upper electrode. The protruding electrode features create locally enhanced electric fields across the capacitor gap that can direct where the pillars form and thus disrupt the natural spacing of the pillars. The natural spacing, however, can only be reduced by a factor of ~ 0.5 since the electric field vectors begin to resemble those of a flat electrode as the protruding features are moved closer together [10].

A careful examination of the parameters that control pillar aspect ratio has shown that the aspect ratio cannot be increased significantly by manipulating parameters in a static setup. Consequently, one of the few conceivable ways to increase the aspect ratio is to physically stretch the pillars, the approach used in this article.

Experimental

Materials

Tris [4-(vinyloxy)butyl] trimellitate ("ene") and pentaerythritol tetrakis(3-mercaptopropionate) ("thiol") were purchased from Aldrich and used as received. A 33 wt% solution of a 1:1 wt mixture of thiol-ene in propylene glycol 1-methyl ether 2-acetate (PGMEA) was spun cast onto doped silicon wafers (functioning as the bottom electrode) to produce $\sim$800-nm films. The low viscosity thiol-ene system is suitable for this study because it forms pillars rapidly at room temperature and is photocurable [5].

Active gap tool

The active gap tool must be able to (i) securely mount a thin-film coated flat substrate; (ii) lower an upper electrode to an assigned, uniform gap without contacting or disrupting the underlying film; (iii) apply an electric field across the gap; (iv) raise the upper electrode in a controllable manner to stretch the pillars; and (v) irradiate the pillars to induce photopolymerization.

Figure 4 is a schematic of the active gap tool. The tool accommodates 4″ wafers mounted rigidly to a ceramic vacuum chuck. The mounted substrate slightly overhangs the edge of the chuck, allowing the substrate to be grounded. The upper electrode (i.e., the template) consists of a 65 × 65 mm, quarter inch thick fused silica template with a centered 1×1 in^2 mesa produced by standard photolithography and etching (Fig. 5). The template must be both transparent and conductive, accomplished by evaporating an $\sim$100 nm coating of indium tin oxide (ITO) onto the surface. The template is vacuum mounted on a flexure ring. The vertical position of the flexure ring is manipulated by three computer-controlled servo motors.

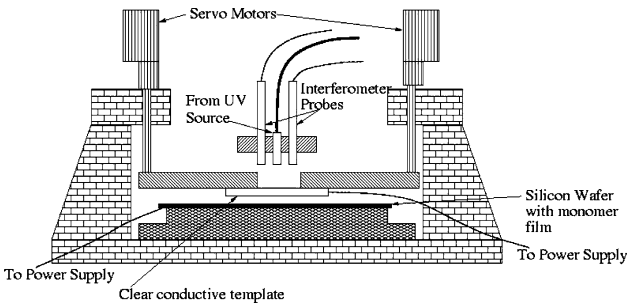

Fig. 4 Labeled illustration of the active gap tool. Only two of the three servo motors and interferometer probes are shown in this cut-away depiction

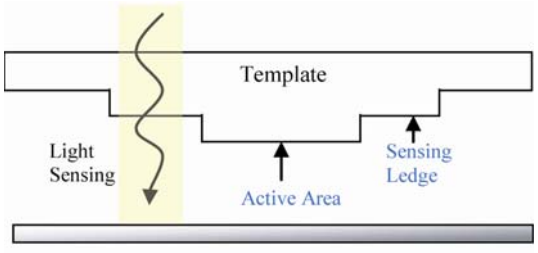

Fig. 5 Side view schematic of the template and the gap monitoring scheme. Light passes through the template and reflects off the substrate. A spectrometer measures the reflected light spectrum to determine the gap thickness. The sensing ledge is typically recessed 0–5 μm from the active area mesa

The gap between the template and the film-coated substrate is monitored by three interferometeric spectroscopy probes. The probes monitor the interference patterns generated by white light reflecting off the substrate. The concept of the gap monitoring scheme is illustrated in Fig. 5. The pillars preferentially form under the active area (i.e., the "mesa") of the template because the electric field is largest there due to the relatively smaller electrode gap. A recessed sensing ledge is used to increase the interferometric signal. Finally, a recessed outer edge is incorporated to prevent the edges of the template from touching the substrate during the template–substrate alignment process.

The active gap tool utilizes pneumatics to coarsely move the substrate/vacuum chuck assembly up and down; this is a requirement for loading and unloading samples. Once loaded, the substrate position is fixed while the template is manipulated by the servo motors with sub-micron resolution to achieve final positioning.

Pillar formation procedure

A thin-film-coated wafer is mounted on the vacuum chuck and grounded. The chuck assembly is rapidly raised pneumatically to within ~100 μm of the template. The template is then lowered to within ~3 μm of the film coated substrate using the servo motors. The entire alignment process is controlled with Lab View®. For gaps below ~3 μm, a protruding active area is utilized (Fig. 5). If the protrusion depth is known, then the final gap is simply the measured gap minus the protrusion depth.

After forming pillars via application of an electric field, the servo motors raise the upper electrode an assigned distance (typically 10–20 μm). The upper electrode is typically raised at a rate of ~100 nm/s. The final gap is measured by interferometery and the pillars are irradiated through the template to induce photopolymerization.

Results and discussion

The active gap tool effectively formed and stretched pillars. Figure 2 is a representative SEM image of an array of thiol-ene pillars formed using the active gap tool without stretching. Figure 6 shows two SEM images of stretched pillar arrays formed using initial starting conditions identical to those used in Fig. 2. A notable fraction of the structures in Fig. 6a are puddles, indicative of pillars that broke as they reached their physical stability limit.

In cases in which the physical stability limit was grossly exceeded prior to UV curing (causing all of the pillars to break), we observed droplets of approximately equal volumes of material on both the upper and bottom electrodes, suggesting that the pillars broke by bifurcation. This observation is consistent with physical intuition since the radius of curvature of the pillars is smallest half way between the upper electrode and the substrate (e.g., Fig. 6b). A bifurcation mechanism is also supported by the geometry of the pillar observed post-stretching. The average diameter of the top of the pillars in Fig. 6 is ~20 μm, which is approximately the same as the average diameter of the non-stretched pillars in Fig. 2; this observation suggests that the middle portion of the pillars contract during stretching to maintain constant volume and eventually reach a point where the structure is no longer stable, resulting in bifurcation.

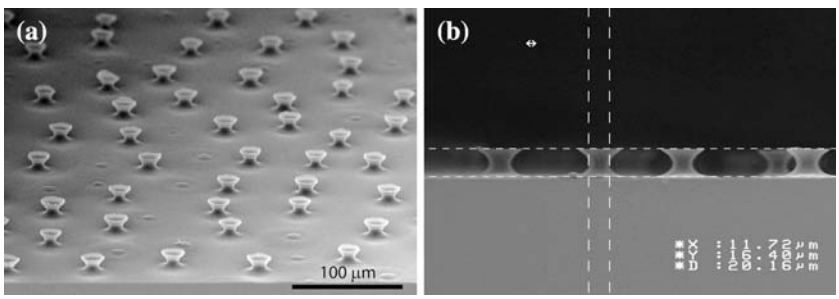

Fig. 6 SEM images of stretched pillars. (**a**) Tilt-view SEM image shows that several of the pillars broke during stretching. (**b**) Side-view SEM shows that pillars stretched to 16.4 μm in height

Stretching limits

At a certain point during stretching, the geometry of the pillar becomes unstable as surface forces conspire to minimize the overall surface energy of the structure. There is a large body of literature on the stability of "liquid bridges"—axisymmetric fluid structures held by surface tension between two surfaces—because of their use in float zone melting. In essence, pillars are liquid bridges that span two flat electrodes; thus the analysis used for liquid bridges is relevant [12].

A perfect cylinder becomes unstable when the aspect ratio reaches π, which is called the Rayleigh–Plateau limit [13, 14]. This theoretical value has been verified experimentally and analysis has been extended to non-cylindrical geometries [15, 16]. The equilibrium shape and stability of a liquid bridge is characterized by both the aspect ratio and the relative volume. The relative volume is the volume of material in the structure divided by the volume of a perfect cylinder defined by the diameter at the base of the column. Liquid bridge stability is determined through analysis of two ordinary differential equations based on the capillary equation and conservation of mass, with boundary conditions dictated by the contact angle [15, 16]. Structures are considered stable if they can withstand small perturbations.

Pillars are constant volume structures that typically have a relative volume less than one (i.e., the pillars have an hour glass shape, as shown in Fig. 6b), implying that the theoretical stability limit will be less than π [12]. Slobozhanin et al. [17] predict that for a liquid bridge with a contact angle of $\sim$35° (the value for the thiol-ene pillars on silicon, estimated by cross-sectional SEM images), the stability will have a maximum aspect ratio between 0.5 and 0.7 for relative volume values between 0.2 and 0.4. Experimentally, the largest aspect ratio thiol-ene pillars obtained by stretching under typical formation conditions ($\sim$3.5 μm initial gap, 40 V, 800 nm initial film) were $\sim$0.5 (Fig. 6).

In situ monitoring of the stretching process (Hawkeye Borescope) verified the stability limit of the pillars. Once $\sim$50% of the pillars broke, we halted the stretching process and photocured the remaining structures. Figure 7 is a side-view SEM image of a pillar with an aspect ratio of $\sim$0.5. The relative volume of the structure in Fig. 7 is $\sim$0.2 based on a 3D integral. Thus, the maximum aspect ratio for this volume fraction is nearly identical to that predicted by theory. Obviously the limit is even larger if the diameter is measured from the narrowest point ($\sim$1.5). The maximum aspect ratio did not vary with the rate of stretching within the range studied (i.e., upper plate retraction rate of 100–500 nm/s).

Electric fields are capable of extending the liquid bridge stability limit [18–20]. However, the theoretical stabilization enhancement is negligible for liquid bridges with the physical parameters associated with pillars [18]. Experimentally, there were no observable differences in the stability limit when stretching with or without electric fields.

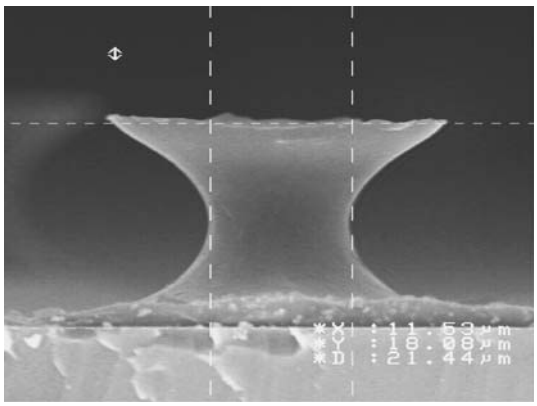

Fig. 7 Side-view SEM of a high-aspect ratio pillar formed by stretching using the active gap tool

Pillars can be stretched beyond the theoretical stability limit by retarding the instability through control of the material properties. This approach is akin to the methods used to draw fibers, in which the aspect ratio of the fibers can begin to approach infinity in continuous processes. Future work will focus on controlling the photocuring process to maximize the aspect ratio through control of the material properties.

Active gap tool capabilities and limits

The two most significant limitations of the active gap tool are (i) the inability to apply heat, which limits the types of materials that can be utilized, and (ii) the inability to apply large electric fields. Large electric fields generate forces that cause the upper electrode assembly to deflect to the lower electrode, which ultimately ruins the experiment. Here, the use of sufficiently low electric fields ($\sim$10 V/μm) minimized deflection, as verified by in situ gap monitoring.

The other limitation of the active gap tool is the minimum achievable gap. It is very difficult to achieve gaps below 2 μm without the use of a sensing ledge, as shown in Fig. 5. The smallest gap to date that successfully formed pillars is $\sim$560 nm, as shown in Fig. 8.

Conclusions

Electrohydrodynamic patterning forms arrays of pillars with low-aspect ratios. The theoretical aspect ratio can be

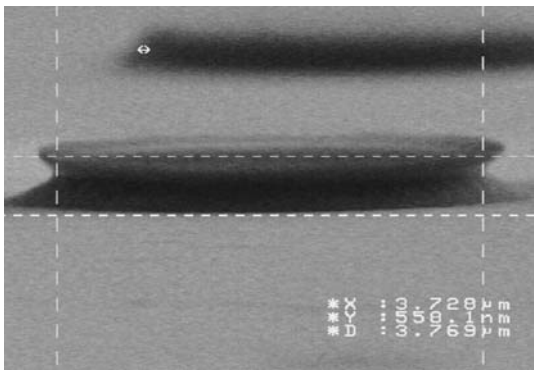

Fig. 8 Tilt-view SEM image of a pillar formed using small electrode gaps ($\sim$560 nm), achieved by using the active gap tool with a sensing ledge template

predicted by combining linear stability analysis with a simple mass balance. Theory suggests stretching the structures post-formation is one of the few ways to increase the aspect ratio of the pillars. We constructed an active gap tool that successfully stretched the pillars. The aspect ratio increased from $\sim$0.1 to $\sim$0.5, which is the theoretical limit for the pillar geometry, as predicted by liquid bridge stability analysis. The aspect ratio can be increased further by retarding the bridge instability via control of the material properties (e.g., by partially curing the polymer prior to exceeding the stability limit), an emphasis of future work.

Acknowledgements The authors thank the Advanced Materials Research Center, the NSF and Intel for graduate fellowships, and the University of Texas CNM for use of the evaporator used to deposit ITO.

References

1. Schaffer E, Thurn-Albrecht T, Russell TP, Steiner U (2000) Nature (London) 403(6772):874
2. Chou SY, Zhuang L (1999) J Vac Sci Technol B 17(6):3197
3. Schaffer E, Thurn-Albrecht T, Russell TP, Steiner U (2001) Europhys Lett 53(4):518
4. Pease LF III, Russel WB (2004) Langmuir 20(3):795
5. Dickey MD, Collister E, Raines A, Tsiartas P, Holcombe T, Sreenivasan SV, Bonnecaze RT, Willson CG (2006) Chem Mater 18(8):2043
6. Herminghaus S (1999) Phys Rev Lett 83(12):2359
7. Pease LF, Russel WB (2003) J Chem Phys 118(8):3790
8. Lin Z, Kerle T, Russell TP, Schaeffer E, Steiner U (2002) Macromolecules 35(10):3971
9. Pease LF, Russel WB (2002) J Non-Newtonian Fluid Mech 102(2):233
10. Verma R, Sharma A, Kargupta K, Bhaumik J (2005) Langmuir 21(8):3710
11. Lin Z, Kerle T, Baker SM, Hoagland DA, Schaffer E, Steiner U, Russell TP (2001) J Chem Phys 114(5):2377
12. Erle MA, Gillette RD, Dyson DC (1970) Chem Eng J 1(1):97
13. Plateau J (1873) Experimentale et Theoretique des Liquides
14. Rayleigh L (1879) Proc R S Lond 29:71
15. Myshkis AD (1987) Low-gravity fluid mechanics: mathematical theory of capillary phenomena. Springer-Verlag, Berlin, New York, pp xix, 583
16. Slobozhanin LA, Perales JM (1993) Phys Fluids A: Fluid Dyn 5(6):1305
17. Slobozhanin LA, Alexander JID, Resnick AH (1997) Phys Fluids 9(7):1893
18. Ramos A, Gonzalez H, Castellanos A (1994) Phys Fluids 6(11):3580
19. Sankaran S, Saville DA (1993) Phys Fluids A: Fluid Dyn 5(4):1081
20. Klingner A, Buehrle J, Mugele F (2004) Langmuir 20(16):6770